REPORT NO. DOT-TSC-FAA-71-11

SIMULATION MODEL FOR THE PIPER PA-30 LIGHT MANEUVERABLE AIRCRAFT IN THE FINAL APPROACH

JOSEPH S. KOZIOL JR.
TRANSPORTATION SYSTEM CENTER
55 BROADWAY
CAMBRIDGE, MA.02142

JULY 1971
TECHNICAL MEMORANDUM

Availability is Unlimited. Document may be Released To the National Technical Information Service, Springfield, Virginia 22151, for Sale to the Public.

Prepared for
FAA/SRDS
800 INDEPENDENCE AVENUE S.W.
WASHINGTON,D.C. 20590

1. Report No.	2. Government Accession No.	3. Recipient's Catalog No.
DOT-TSC-FAA-71-11		

4. Title and Subtitle	5. Report Date
SIMULATION MODEL FOR THE PIPER PA-30 LIGHT MANEUVERABLE AIRCRAFT IN THE FINAL APPROACH	June, 1971
	6. Performing Organization Code
7. Author(s) Joseph S. Koziol, Jr.	8. Performing Organization Report No.
9. Performing Organization Name and Address TRANSPORTATION SYSTEMS CENTER 55 BROADWAY CAMBRIDGE, MASS. 02142	10. Work Unit No.
	11. Contract or Grant No.
12. Sponsoring Agency Name and Address FAA/SRDS 800 Independence Avenue, S. W. Washington, D. C. 20590	13. Type of Report and Period Covered TECHNICAL MEMORANDUM
	14. Sponsoring Agency Code

15. Supplementary Notes

16. Abstract

This report describes the Piper PA-30 "Twin Comanche" aircraft and a representative autopilot during the final approach configuration for simulation purposes. The aircraft is modeled by linearized six-degree-of-freedom perturbation equations referenced to the aircraft stability axis. Other equations are presented which derive the body axis rates, velocities and accelerations, and ground referenced velocities (translation equations).

The autopilot is a representative system for automatic ILS approaches from initial localizer track down to decision height. The glideslope system is engaged by approaching the glidepath at constant altitude (usually in the altitude hold mode) on the localizer beam. The pilot must take over manually at the decision height since light aircraft are not normally equipped with automatic flare capability.

The aircraft autopilot model described herein has been used extensively in simulation studies at TSC and exhibits the expected behavior.

17. Key Words	18. Distribution Statement
Light maneuverable aircraft, autopilot model, final approach, simulation studies	Unclassified - Unlimited

19. Security Classif. (of this report)	20. Security Classif. (of this page)	21. No. of Pages	22. Price
Unclassified	Unclassified	21	

The contents of this report reflect the views of the Federal Aviation Administration which is responsible for the facts and the accuracy of the data presented herein. The contents do not necessarily reflect the official views or policy of the Department of Transportation. This report does not constitute a standard, specification or regulation.

TABLE OF CONTENTS

LIST OF ILLUSTRATIONS

SYMBOLS

a_n	measured normal acceleration at accelerometer station	ft/sec^2
b	wing span	ft.
BHP	engine brake horsepower	-
c	mean aerodynamic chord	ft.
C_D	drag coefficient	-
$C_{D()}$	nondimensional drag stability derivative	-
$C_{ha()}$	nondimensional aileron hinge-moment coefficient	-
$C_{he()}$	nondimensional elevator hinge-moment coefficient	-
$C_{hr()}$	nondimensional rudder hinge-moment coefficient	-
C_L	lift coefficient	-
$C_{L()}$	nondimensional lift stability derivative	-
C_ℓ	rolling-moment coefficient	-
$C_{\ell()}$	nondimensional rolling-moment stability derivative	-
C_m	pitching-moment coefficient	-
$C_{m()}$	nondimensional pitching-moment stability derivative	-
C_n	yawing-moment coefficient	-
$C_{n()}$	nondimensional yawing-moment stability derivative	-
C_Y	side-force coefficient	-
$C_{Y()}$	nondimensional side-force stability derivative	-

C_T	thrust coefficient	-
g	gravity constant	ft/sec^2
h	aircraft altitude referenced to sea level	ft.
$I_{xx()}$	aircraft rolling moment of inertia	$slug\text{-}ft^2$
$I_{yy()}$	aircraft pitching moment of inertia	$slug\text{-}ft^2$
$I_{zz()}$	aircraft yawing moment of inertia	$slug\text{-}ft^2$
$I_{xz()}$	aircraft product of inertia	$slug\text{-}ft^2$
m	mass of aircraft	slugs
MAP	engine absolute manifold pressure	in. of Hg
N_P	engine power efficiency	-
$p_{()}$	rolling angular rate of aircraft (about stability axis when no subscript)	rad/sec
$q_{()}$	pitching angular rate of aircraft (about stability axis when no subscript)	rad/sec
$\bar{q}$	free-stream dynamic pressure	lbs/ft^2
r	yawing angular rate of aircraft (about stability axis when no subscript)	rad/sec
r.p.m.	engine revolutions per minute	-
S	wing area	ft^2
T	effective thrust	lbs.
ΔT	change in thrust due to pilot throttle input	lbs.
$u_{()}$	perturbed forward velocity of aircraft (along stability x-axis when no subscript)	ft/sec
U_o	equilibrium or reference forward velocity of aircraft	ft/sec
$v_{()}$	perturbed side velocity of aircraft (along atability Y-axis when no subscript)	ft/sec
V_T	total velocity of aircraft	knots

$w_{()}$	perturbed normal velocity of aircraft (along stability Z axis when no subscript)	ft/sec
x_{accel}	distance from center of gravity to accelerometer location measured along X fuselage axis, positive forward	ft.
X_E	X-axis in local vertical coordinate frame	-
Y_E	Y-axis in local vertical coordinate frame	-
Z_E	Z-axis in local vertical coordinate frame	-
Z_T	pitching moment arm of the thrust vector positive downward	ft.
α	angle of attack = $\tan^{-}(w/u)$	rad.
α_r	angle between X-stability axis and fuselage axis	rad.
α_T	angle between X-stability axis and thrust axis	rad.
β	angle of sideslip = $\sin^{-}(v/V_T)$	rad.
ε	glideslope error, localizer error	rad.
δ_t	deflection of throttle position (δ_t = 1 = full throttle)	-
$\delta_{()}$	deflection of control surface	rad.
θ,ϕ,ψ	Euler angles referenced to stability axis	rad.
ρ	atmospheric air density	slug/ft^3
$(\dot{\ })$	derivative with respect to time	-

Subscripts

a	aileron
B	fuselage reference frame
E	local vertical coordinate frame
e	elevator or stabilizer
f	flaps

o	equilibrium or reference condition
r	rudder
s	aircraft stability coordinate frame
t	throttle
$u, \alpha, q, \beta, r, p\ \delta_e, \delta_a, \delta_r$	as defined above

1.0 INTRODUCTION

The primary objective of this research effort is to derive a light, maneuverable aircraft-autopilot model as one extreme of aircraft type for final approach simulation studies. This model is to serve as a high priority vehicle in two FAA projects: developing requirements for a Scanning Beam Microwave Instrument Landing System and developing an all-encompassing generalized set of equations of an aircraft during approach and landing for all-weather landing system studies on the NAFEC hybrid computation facility.

In general, no such model existed for a common and representative light aircraft at the beginning of this effort because light aircraft are not generally designed by analysis and simulation. Similarly, light aircraft generally do not have automatic landing systems as standard equipment.

The definition and identification of a light maneuverable aircraft is treated in Reference (1). The Piper PA-30 "Twin Comanche" is selected as the light maneuverable aircraft for modeling primarily because of the availability of data from wind tunnel and actual flight tests and because of an existing, partially useful, simulation model at the NASA Edwards Flight Research Center. The final aircraft model is derived from this simulation model and NASA TN D4983. The flight condition is based upon a high wind environment (headwind and sidewind of approximately 24 feet per second). This condition was selected to represent an extreme case for the simulation studies.

The autopilot description is based on a report (Reference 6) prepared for TSC by Dr. Kohlman of the University of Kansas. The final configuration (i.e., gain values, gain scheduling and logic) was determined by simulation at TSC.

2.0 VEHICLE DESCRIPTION [4]

The Piper PA-30 is a light twin engine low-wing monoplane. Figure 1 gives the principal dimensions. The airplane has a wing span of 35.98 ft., a wing area of 178 ft^2, an aspect ratio of 7.3, and a mean aerodynamic cord of 5 feet based on projection of the outboard leading edge of the wing through the fuselage. The wing airfoil section is a modified $NACA64_2A215$ airfoil with the trailing-edge cusp faired out. The wing has 5° of dihedral with no twist and is at 2° positive incidence with respect to the fuselage reference line. The airplane has the standard three-control system. The horizontal tail is of the all-movable type with a control deflection range of 4° to -14°. The tail has a trailing-edge tab which moves in the same direction as the tail with a deflection ratio (tab deflection to tail deflection) of 1.5. The control deflection range on each aileron is from 14° to -18°. The rudder control deflection range is ±27°.

2.1 Vehicle Model

A final approach model is presented for the Piper PA-30 aircraft based on data available from the NASA Edwards Flight Research Center simulation model and NASA TND 4983. The model consists of rigid body, six-degree-of-freedom aircraft equations of motion which are basically linear perturbation equations in the stability axis system (some of the nonlinear cross coupling terms have been included).

2.2 Axis Systems

The stability axis frame (s) is depicted in Figure 2. The definition of airplane angles and sign convention is described in Figure 3. The stability axis is fixed to the aircraft and rotates and translates with the aircraft. Its origin is the center of mass of the aircraft. The X-axis is in the direction of motion of the airplane in a reference condition of steady

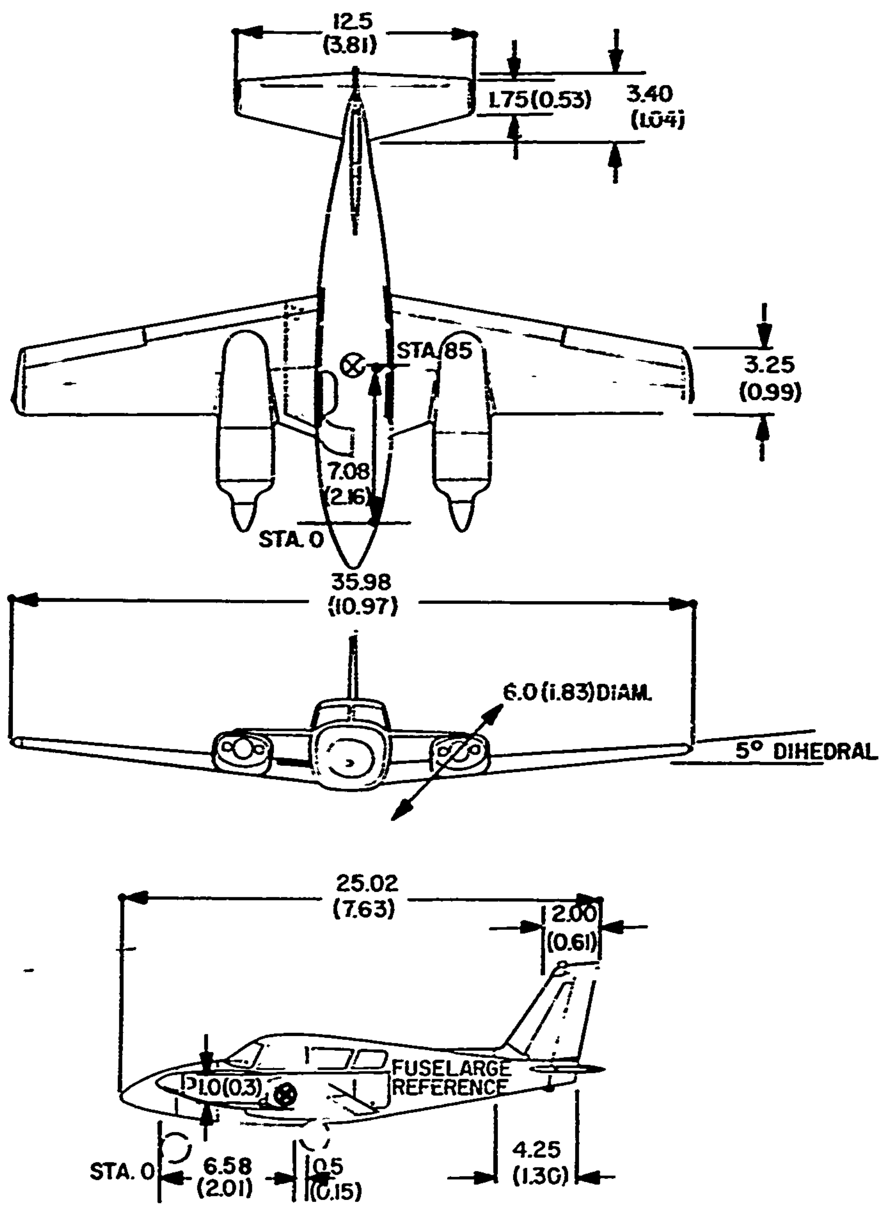

All dimensions are in feet (meters).

Figure 1. Piper Dimensional Data[4]

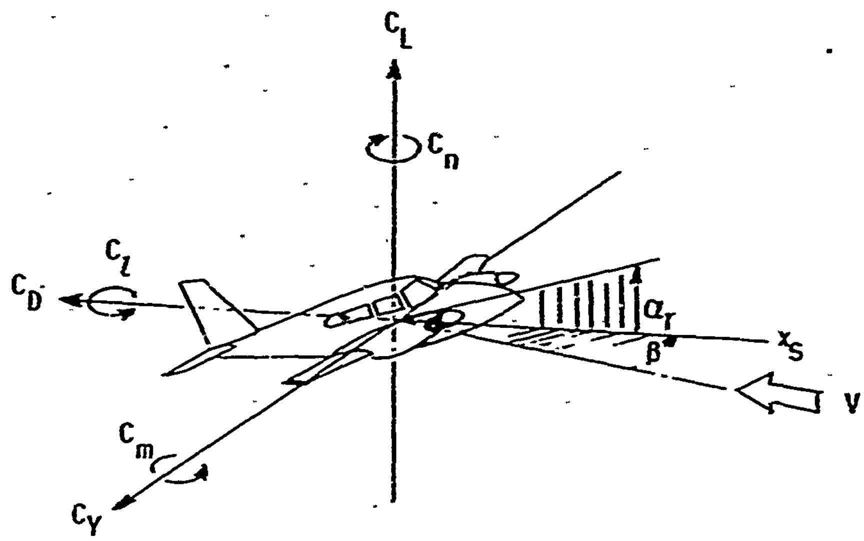

Figure 2. System of Axes and Positive Sense of Angles, Forces and Moments[4]

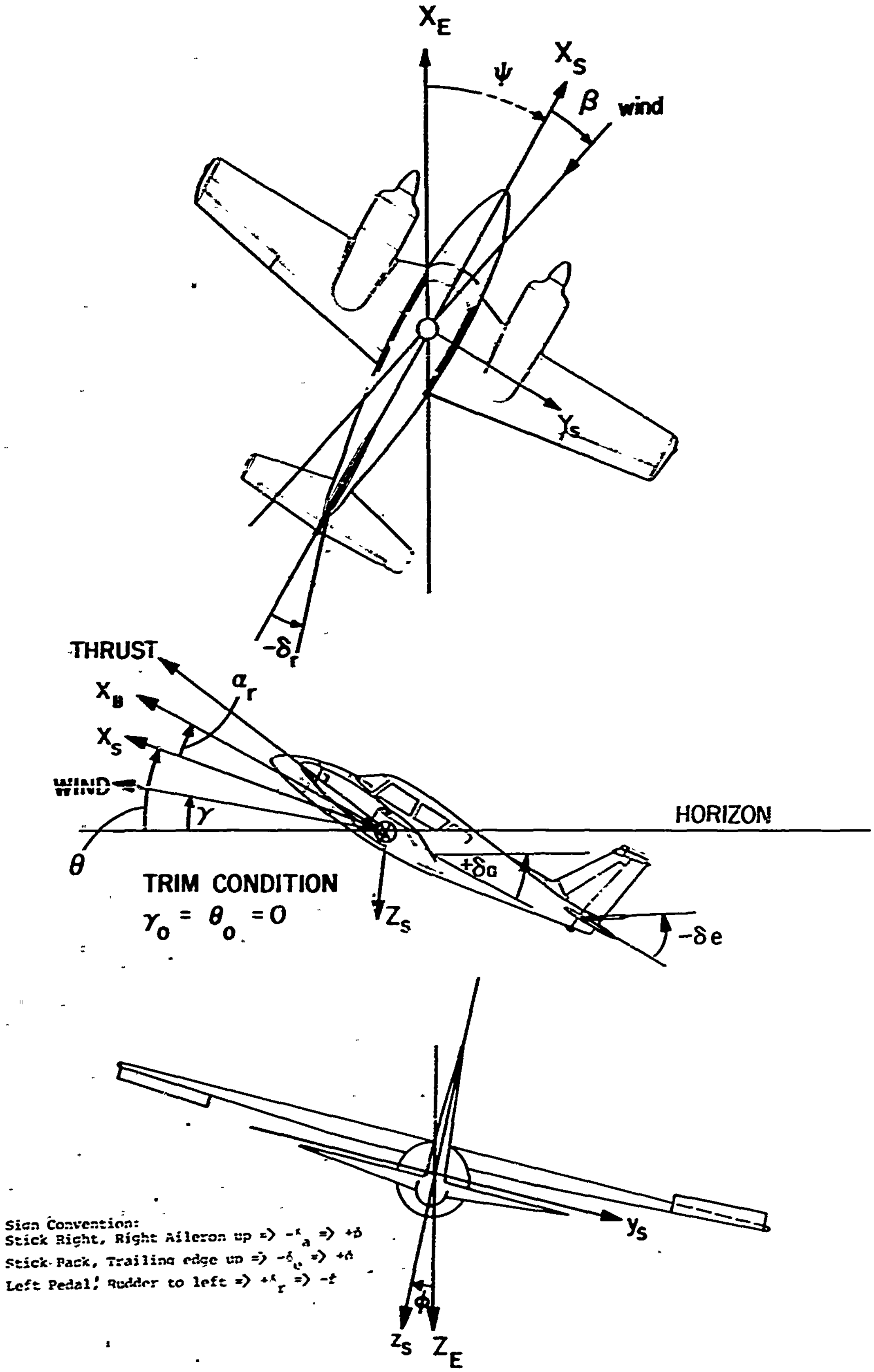

Figure 3. Definition of Airplane Angles and Sign Convention

symmetric flight. The Y-axis is normal to the aircraft's plane of symmetry (positive to the right), and the Z-axis is in the plane of symmetry (positive downward) and orthogonal to the X- and Z-axes. The aerodynamic stability derivatives are all referenced to this axis system.

A fuselage referenced body coordinate frame (B), is defined for determining the angular rates and velocities in body axis, and the aircraft normal acceleration. This axis system is similar to the stability axis system except that the X-axis is directed along the fuselage. The angle α_r relates the two axis systems. A local vertical coordinate frame (E) is defined for determining the velocities of the aircraft with respect to the air mass. This coordinate frame has its origin at the center of mass of the aircraft with the X-axis pointing North, and Y-axis pointing East, and the Z-axis pointing down. The velocities from this coordinate frame can be converted to ground velocity by adding the various components of the steady wind.

2.3 Assumptions in Using Aircraft Equations

The derivation of the aircraft equations involved the following assumptions:

1. Aircraft mass is constant.
2. The earth can be considered an inertial frame.
3. The aircraft is a rigid body.
4. The aircraft is symmetrical about its X-Z plane.
5. The aircraft is initially in equilibrium flight with no linear or angular accelerations, no angular rates, and no initial roll angle or lateral velocity.
6. Small disturbance (perturbation) theory is used. Motions and forces are referred to the equilibrium flight condition.
7. Hinge moments are insignificant.

2.4 Equations of Motion

Drag Equation

$$\frac{m}{\bar{q}S}\dot{u} + \frac{2C_{D_o}}{U_o}u - \left(C_{L_o} - C_{D_\alpha}\right)\alpha + \frac{mg}{\bar{q}S}\theta - \frac{mU_o}{\bar{q}S}r\beta = \left(\frac{\cos\alpha_T}{\bar{q}S}\right)\Delta T$$

Lift Equation

$$\frac{2C_{L_o}}{U_o}u + \left(\frac{mU_o}{\bar{q}S} + \frac{c}{2U_o}C_{L_{\dot{\alpha}}}\right)\dot{\alpha} + \left(C_{L_\alpha} + C_{D_o}\right)\alpha + \left(\frac{c}{2U_o}C_{L_q} - \frac{mU_o}{\bar{q}S}\right)q$$

$$+ \left(\frac{mg}{\bar{q}S}\theta_o\right)\theta + \frac{mU_o}{\bar{q}S}\beta p - \frac{m}{\bar{q}S}qu = -C_{L_{\delta_e}}\delta_e - \left(\frac{\sin\alpha_T}{\bar{q}S}\right)\Delta T$$

Pitching Moment Equation

$$-\frac{C_{m_u}}{U_o}u - \frac{c}{2U_o}C_{m_{\dot{\alpha}}}\dot{\alpha} - C_{m_\alpha}\alpha + \frac{I_{yy_S}}{\bar{q}Sc}\dot{q} - \frac{c}{2U_o}C_{m_q}q = C_{m_{\delta_e}}\delta_e + \frac{z_T}{\bar{q}Sc}\Delta T$$

Sideforce Equation

$$\frac{mU_o}{\bar{q}S}\dot{\beta} - C_{Y_\beta}\beta - \frac{b}{2U_o}C_{Y_p}p - \frac{mg}{\bar{q}S}\phi + \frac{mU_o}{\bar{q}S}r - \frac{b}{2U_o}C_{Y_r}r + \frac{m}{\bar{q}S}ru =$$

$$C_{Y_{\delta r}}\delta r + C_{Y_{\delta a}}\delta a$$

Rolling Moment Equation

$$-C_{\ell_\beta}\beta + \frac{I_{xx_S}}{\bar{q}Sb}\dot{p} - \frac{b}{2U_o}C_{\ell_p}p - \frac{I_{xz_S}}{\bar{q}Sb}\dot{r} - \frac{b}{2U_o}C_{\ell_r}r = C_{\ell_{\delta r}}\delta r + C_{\ell_{\delta a}}\delta a$$

Yawing Moment Equation

$$-C_{n_\beta}\beta - \frac{I_{xz_S}}{\bar{q}Sb}\dot{p} - \frac{b}{2U_o}C_{n_p}p + \frac{I_{zz_S}}{\bar{q}Sb}\dot{r} - \frac{b}{2U_o}C_{n_r}r = C_{n_{\delta_r}}\delta r + C_{n_{\delta_a}}\delta a$$

Body Axis Rates and Velocities

$$q_B = q$$

$$p_B = p \cos(\alpha_r) - r \sin(\alpha_r)$$

$$r_B = r \cos(\alpha_r) + p \sin(\alpha_r)$$

$$u_B = (U_o + u) \cos(\alpha_r) - U_o\alpha \sin(\alpha_r)$$

$$w_B = U_c\alpha \cos(\alpha_r) + (U_o + u) \sin(\alpha_r)$$

$$v_B = U_o\beta$$

Accelerations

Vertical acceleration at center of gravity

$$\dot{w}_B = U_o\dot{\alpha} \cos(\alpha_r) + \dot{u} \sin(\alpha_r)$$

Vertical acceleration at accelerometer

$$\dot{w}_{accel} = \dot{w}_B - x_{accel}\,\dot{q}$$

Measured Normal Acceleration

$$a_n = \dot{w}_{accel} + p_B v_B - q_B U_B$$

Euler Angle Rates

$$\dot{\theta} = q \cos \Phi - r \sin \Phi$$

$$\dot{\Phi} = p + (q \sin \Phi + r \cos \Phi) \tan \theta$$

$$\dot{\Psi} = (q \sin \Phi + r \cos \Phi) \sec \theta$$

Translation Equations With Respect to Moving Frame

$$\dot{X}_E = (U_o+u)\cos\theta\cos\psi + U_o\beta(\sin\Phi\sin\theta\cos\psi - \cos\Phi\sin\psi) + U_o\alpha(\cos\Phi\sin\theta\cos\psi + \sin\Phi\sin\psi)$$

$$\dot{Y}_E = (U_o+u)\cos\theta\sin\psi + U_o\beta(\sin\Phi\sin\theta\sin\psi + \cos\Phi\cos\psi) + U_o\alpha(\cos\Phi\sin\theta\sin\psi - \sin\Phi\cos\psi)$$

$$\dot{Z}_E = (U_o+u)(-\sin\theta) + U_o\beta\sin\Phi\cos\theta + U_o\alpha\cos\Phi\cos\theta.$$

2.5 Vehicle Data

Geometry

$b = 35.98$ ft.

$c = 5.$ ft.

$S = 178.$ ft.^{2}

$Z_T = -.75$ ft.

$\alpha_T = 0$ deg.

Weight and Inertias

$m = 111.9$ slugs	$I_{xxB} = 2800$ slug-ft^2	$I_{xxs} = 2801.7$ slug-ft^2
	$I_{yyB} = 1900$ slug-ft^2	$I_{yys} = 1900.$ slug-ft^2
	$I_{zzB} = 4500$ slug-ft^2	$I_{zzs} = 4513.7$ slug-ft^2
	$I_{xzB} = 80$ slug-ft^2	$I_{xzs} = -7.9$ slug-ft^2

Trim Flight Condition - Final Approach(High Wind Environment)

$U_o = 176.$ ft/sec

$C_{Lo} = .55$

$C_{Do} = .034$

$\theta_o = 0.^\circ$

$\gamma_o = 0.^\circ$

δ_e (trim elevator setting) $= 0.4^\circ$

δ_f (trim flap setting) $= 0.^\circ$

$\rho = .002378$ slugs/ft^3

$\bar{q} = 36.8$ lbs/ft^2

$\alpha_r = .0515$ rad (2.95°)

C_T (thrust coeff.) $\cong .034$

center of gravity at 10% MAC
gear down

Non-Dimensional Derivatives - Final Approach

$C_{D_u} = 0.$	$C_{L_u} = 0.$	$C_{m_u} = 0.$
$C_{D_\alpha} = .275$	$C_{L_\alpha} = 5.04$	$C_{m_\alpha} = -1.147$
$C_{D_{\dot\alpha}} = 0.$	$C_{L_{\dot\alpha}} = 5.3$	$C_{m_{\dot\alpha}} = -14.55$
$C_{D_q} = 0.$	$C_{L_q} = 9.12$	$C_{m_q} = -25.0$
$C_{D_{\delta e}} = 0.$	$C_{L_{\delta e}} = 1.05$	$C_{m_{\delta e}} = -2.87$
$C_{\ell_\beta} = -.086$	$C_{n_\beta} = .0756$	$C_{Y_\beta} = -.494$
$C_{\ell_r} = .11$	$C_{n_r} = -.16$	$C_{Y_r} = 0.$
$C_{\ell_p} = -.50$	$C_{n_p} = -.063$	$C_{Y_p} = 0.$
$C_{\ell_{\delta r}} = .01147$	$C_{n_{\delta r}} = -.0573$	$C_{Y_{\delta r}} = .143$
$C_{\ell_{\delta a}} = -.0803$	$C_{n_{\delta a}} = .00573$	$C_{Y_{\delta a}} = -.00916$

2.6 Control Wheel and Pedal Characteristics

Aileron: Gearing constant at zero control deflection, 0.80 radian/ft.; wheel deflection, $\pm 90^\circ$; max. force at end of wheel, ± 15 lb.

Elevator: Gearing constant at zero control deflection, 0.42 radian/ft.; wheel throw, 4 inches forward, 5 inches aft; force differential 40 lbs. (detent position is 4 inches from firewall)

Rudder: Gearing constant at zero control deflection, 0.93 radian/ft.; pedal deflection, 4 1/2 inches; maximum force at full deflection, 120 lbs.

3. ENGINE THRUST DATA

Two 160 h.p. Lycoming IO-320-B four-cylinder air-cooled engines power the PA-30. Figure 4 presents the maximum available manifold pressure from each engine as a function of standard temperature altitude. This curve should be mechanized so that the pilot's indicator shows the maximum value as a function of altitude at full throttle.

Figure 5 presents the power available per engine as a function of r.p.m., MAP, and altitude. This curve should be mechanized so that power can be obtained from the r.p.m., MAP, and altitude.

Once the power is obtained, thrust can be calculated from the following equation:

$$T\ (\text{lbs.}) = \frac{325\ N_P\ BHP}{V_T\,(\text{knots})}$$

where N_P (power efficiency) = 0.74

Alternatively, a simplified algebraic expression for BHP has been derived from Figure 5 for the final approach configuration and can be used in place of Figure 5. The expression is given by

$$BHP = .0024(h) + .0028(\text{r.p.m.}) \left\{ \left[\delta_t \left(29.2 - .000989(h) \right) \right] - 8.0 \right\}$$

where h = altitude in feet

δ_t = 1 = full throttle

An engine lag of about 0.1 second can be used in completing the engine transfer function (i.e. throttle→thrust).

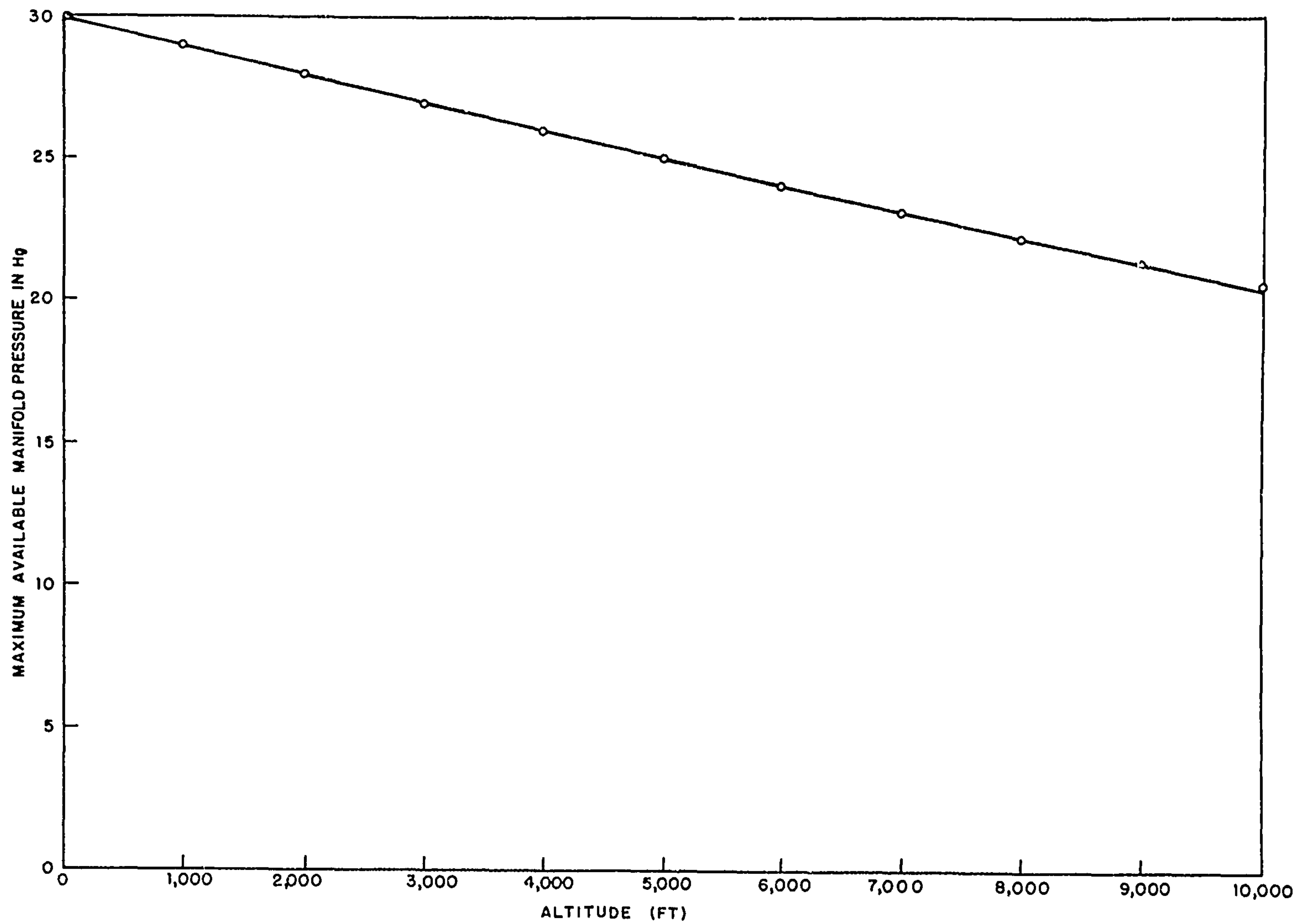

Figure 4. Maximum Available Manifold Pressure

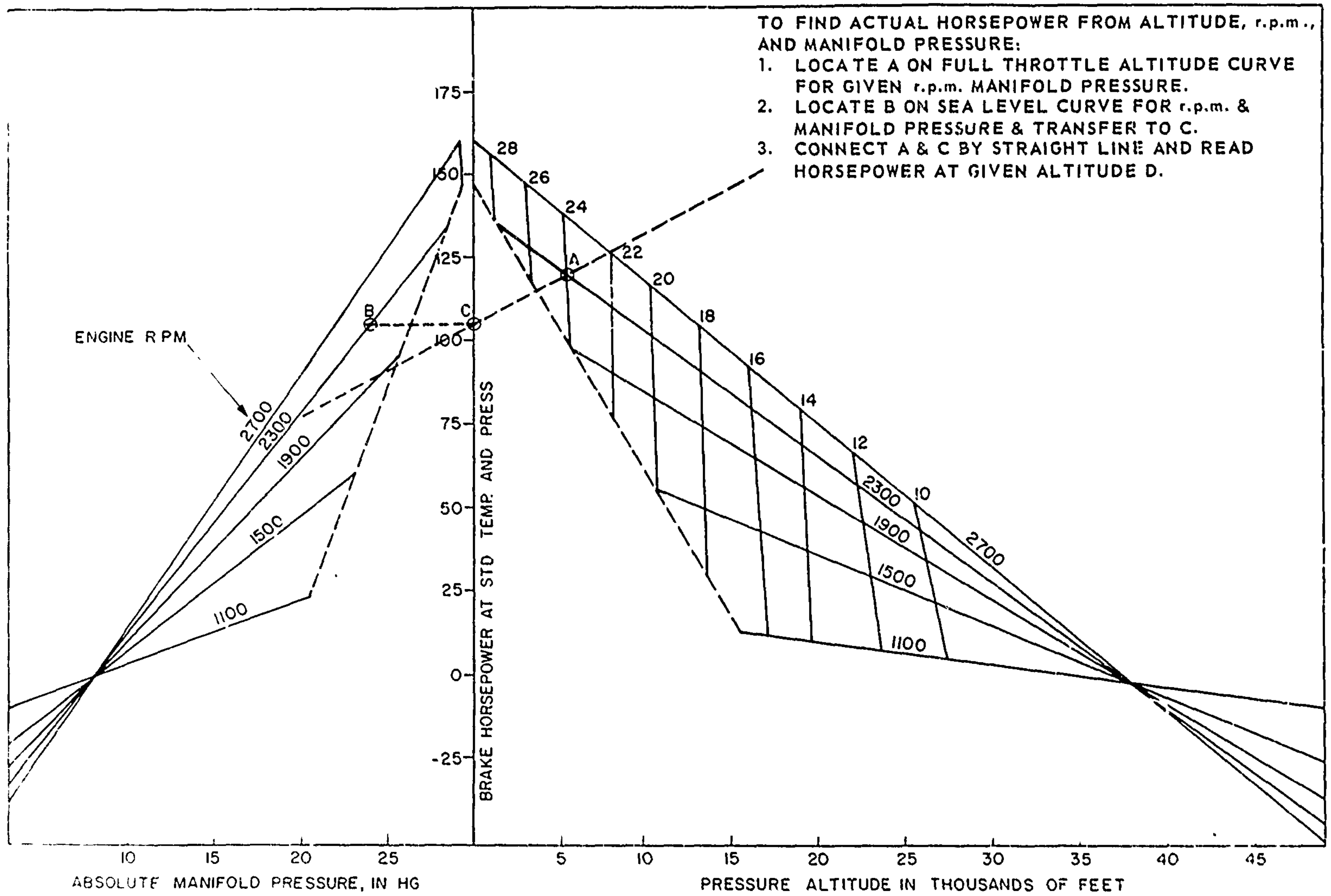

Figure 5. Power Characteristics Per Engine

4. AUTOPILOT

This section describes a representative PA-30 three-axis autopilot with stabilization system and with an automatic ILS approach mode available down to decision height.

Block diagrams of the longitudinal and lateral axis are shown in Figures 6 and 7 respectively. Damping is provided about all three axes, and inputs to the system come from a vertical gyro (θ, Φ), yaw rate gyro (r), altitude sensor, and navigation receiver. Limiters are installed in the lateral channel to prevent excessive roll angles in response to large error signals. Gain scheduling is provided in the longitudinal channel to desensitize the system to glidepath errors as the runway threshold is approached. Automatic ILS approaches are possible down to decision height. The pilot must take over manually at that point because there is no automatic flare capability.

The auto-trim system, which actuates the elevator trim tab to unload the elevator servo, is not included in the block diagrams since it has no measurable influence on the performance or dynamic response of the airplane-autopilot system. It is a time-delayed, slow, integrating actuator and as such does not respond to transients.

The output of the autopilot system is expressed in control surface deflections. Because of the dependence of deflections on dynamic pressure, the final gain of $1/\bar{q}$ represents the aerodynamic gain of the control surfaces.

The glideslope system is engaged by approaching the glidepath at constant altitude (usually in the altitude hold mode) on the localizer beam. Initially the glideslope error signal will be a strong nose up command but switch B will be open. The "glideslope engage logic" circuit continuously monitors the signal at point B, which will gradually decrease in strength as the glidepath is approached. When the signal at point B reaches a 0.044 rad. (2.5°) nose up command, switch B is closed, and the altitude hold mode is

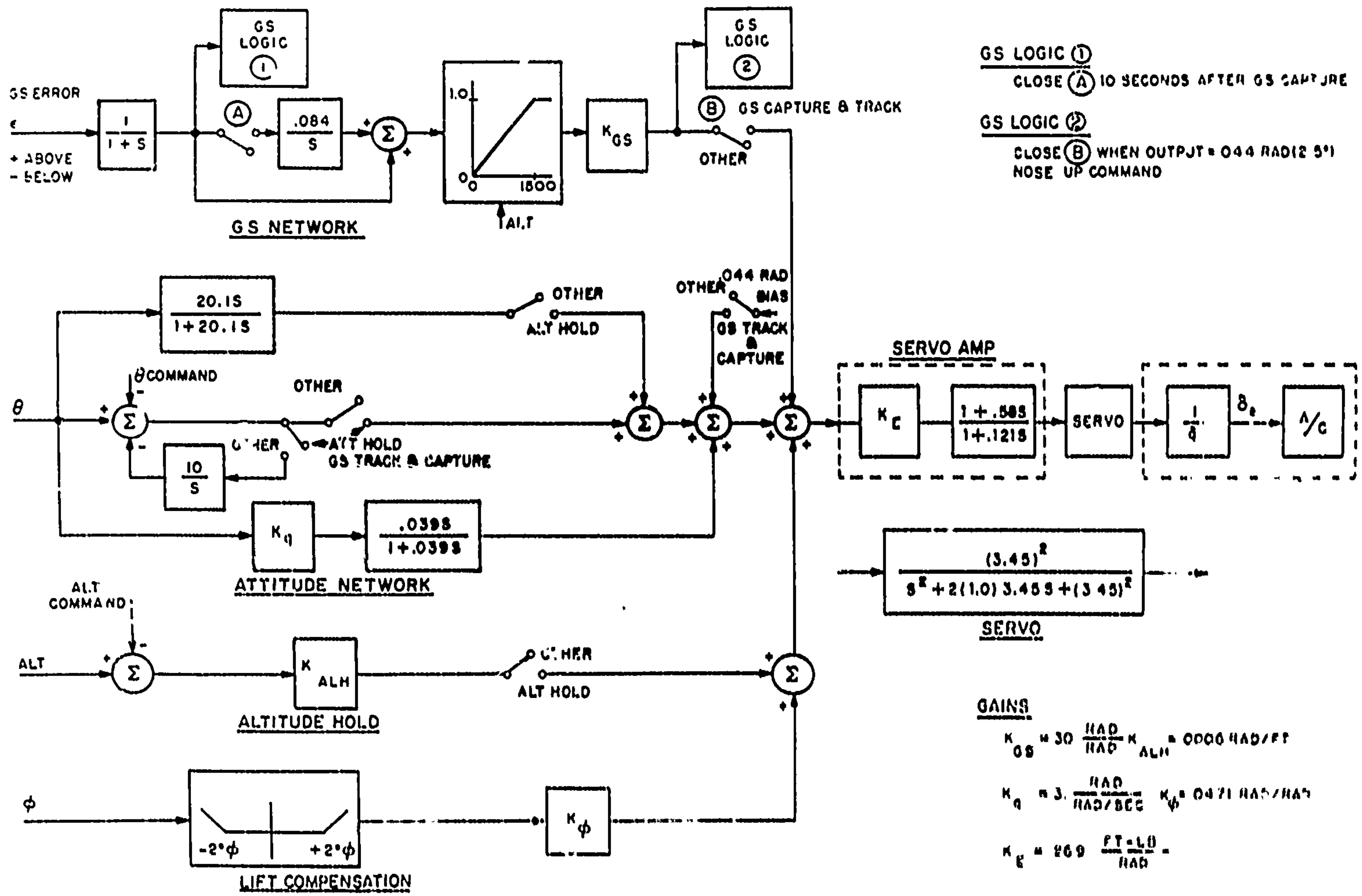

Figure 6. Longitudinal Control System

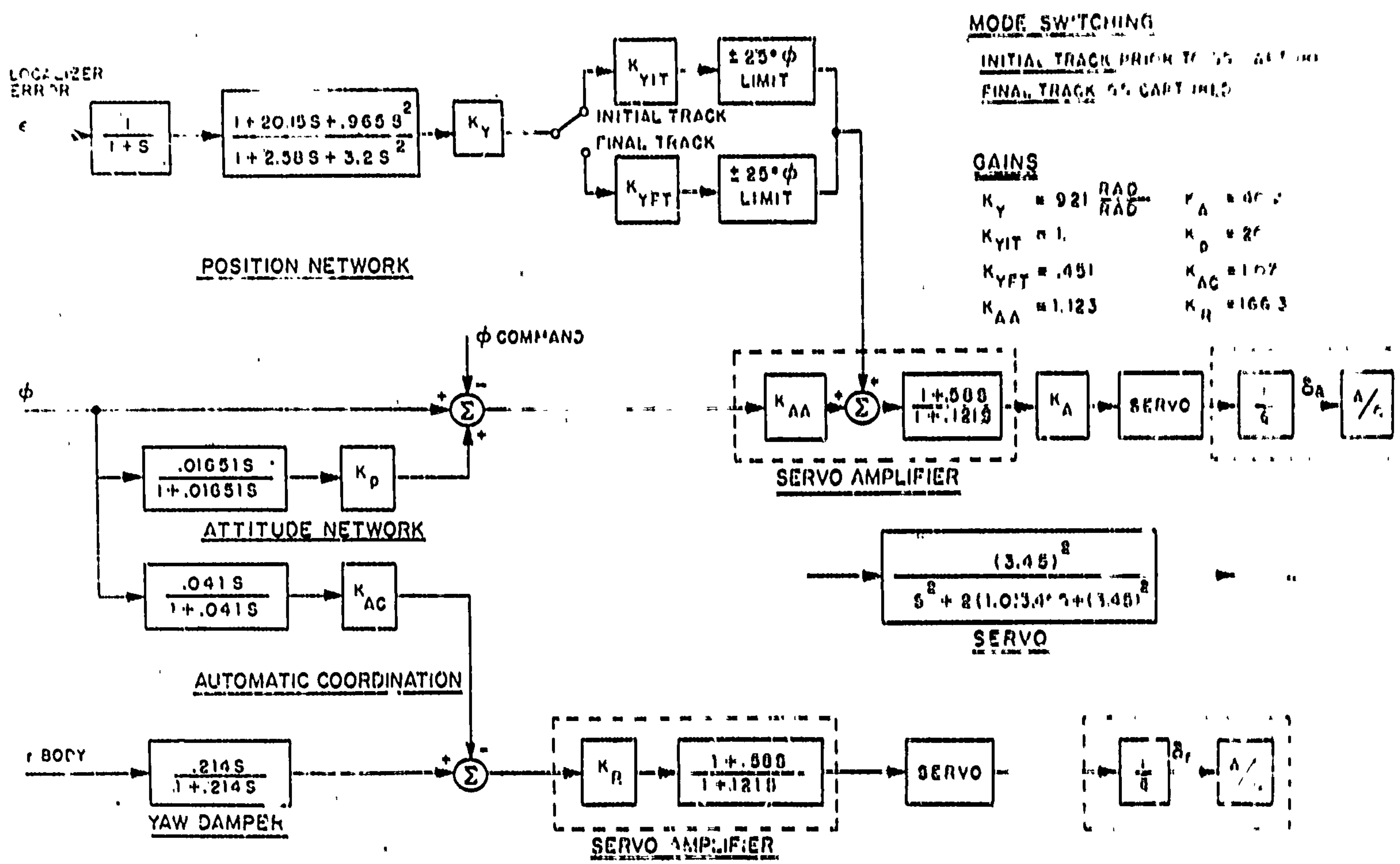

Figure 7. Lateral Control System

disengaged. To prevent a sudden pitchup at this point a 0.044 rad. nose down command is biased into the attitude circuit, to cancel the input from switch B. Thus, after engagement, the airplane will continue in level flight. As it moves closer to the glidepath, the signal at B will continue to decrease, and the bias signal will gradually pitch the nose down. The gains and logic switches are set so that the airplane gradually approaches the correct glideslope with minimal overshoot. Speed is controlled manually at all times in the representative autopilot system since auto-throttles are not typically provided. However, a preliminary auto-throttle was derived at TSC by simulation and can be used for completely automatic approach studies. The auto-throttle system is shown in Figure 8.

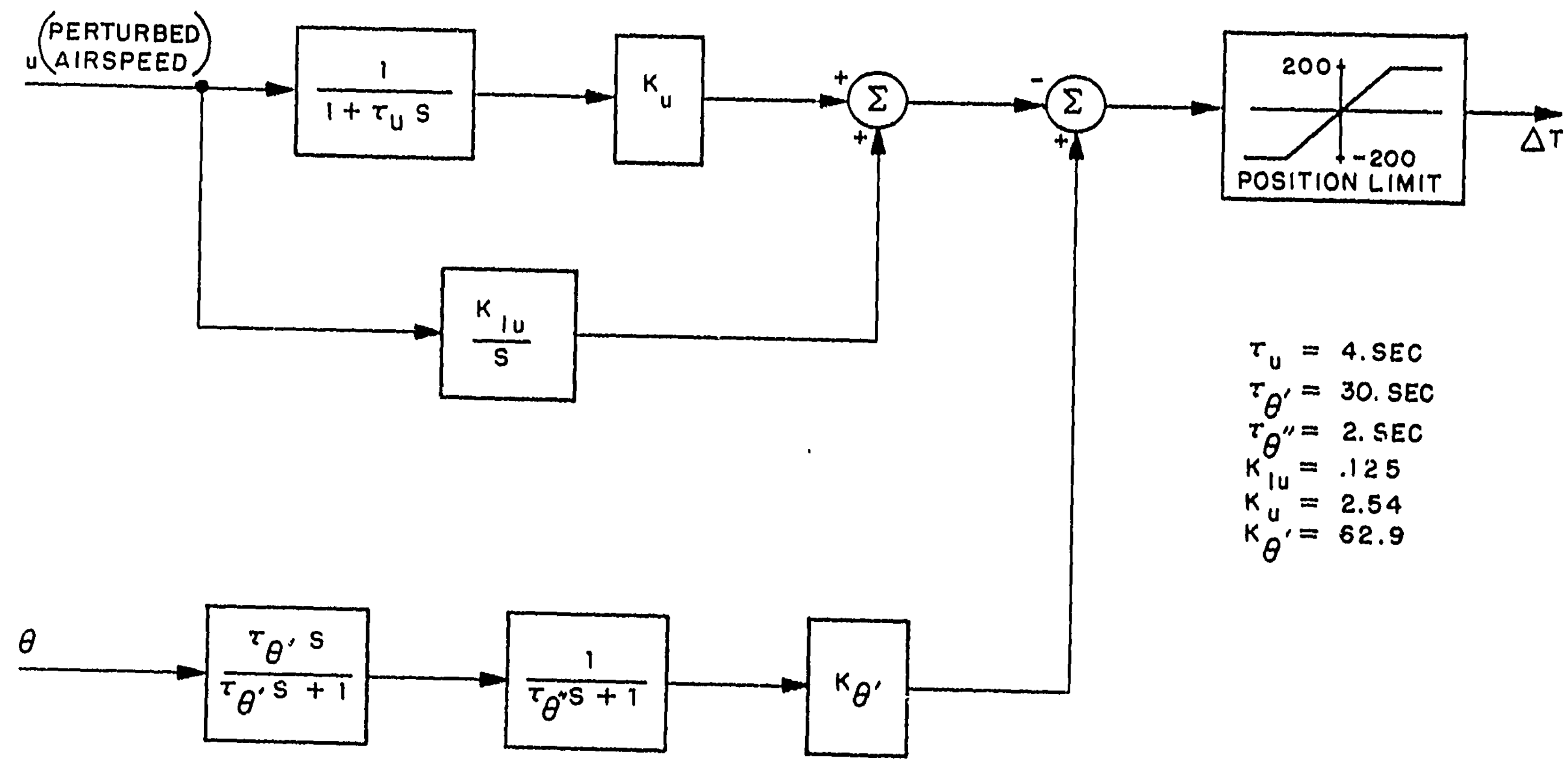

Figure 8. Auto-throttle

5. INSTRUMENT PANEL[5]

The instrument panel layout is shown in Figure 9. It is designed to accommodate the customary advanced flight instruments on the left side in front of the pilot and engine instruments on the right side.

1. RATE OF TURN INDICATOR
2. AIRSPEED INDICATOR
3. STALL WARNING LIGHT
4. GYRO HORIZON
5. G/S COUPLER LIGHT
6. DIRECTIONAL GYRO
7. ALTIMETER
8. RATE OF CLIMB
9. OMNI BEARING SELECTOR
10. MARKER BEACON
11. TRANSPONDER
12. RADIO SELECTOR PANEL
13. ADF RADIO
14. COMM/NAV TRANSCEIVERS
15. ALTIMATIC IIIB
16. LEFT TACHOMETER
17. MANIFOLD PRESSURE GAUGE
18. RIGHT TACHOMETER
19. FUEL FLOW INDICATOR
20. FUEL AND ENGINE GAUGES

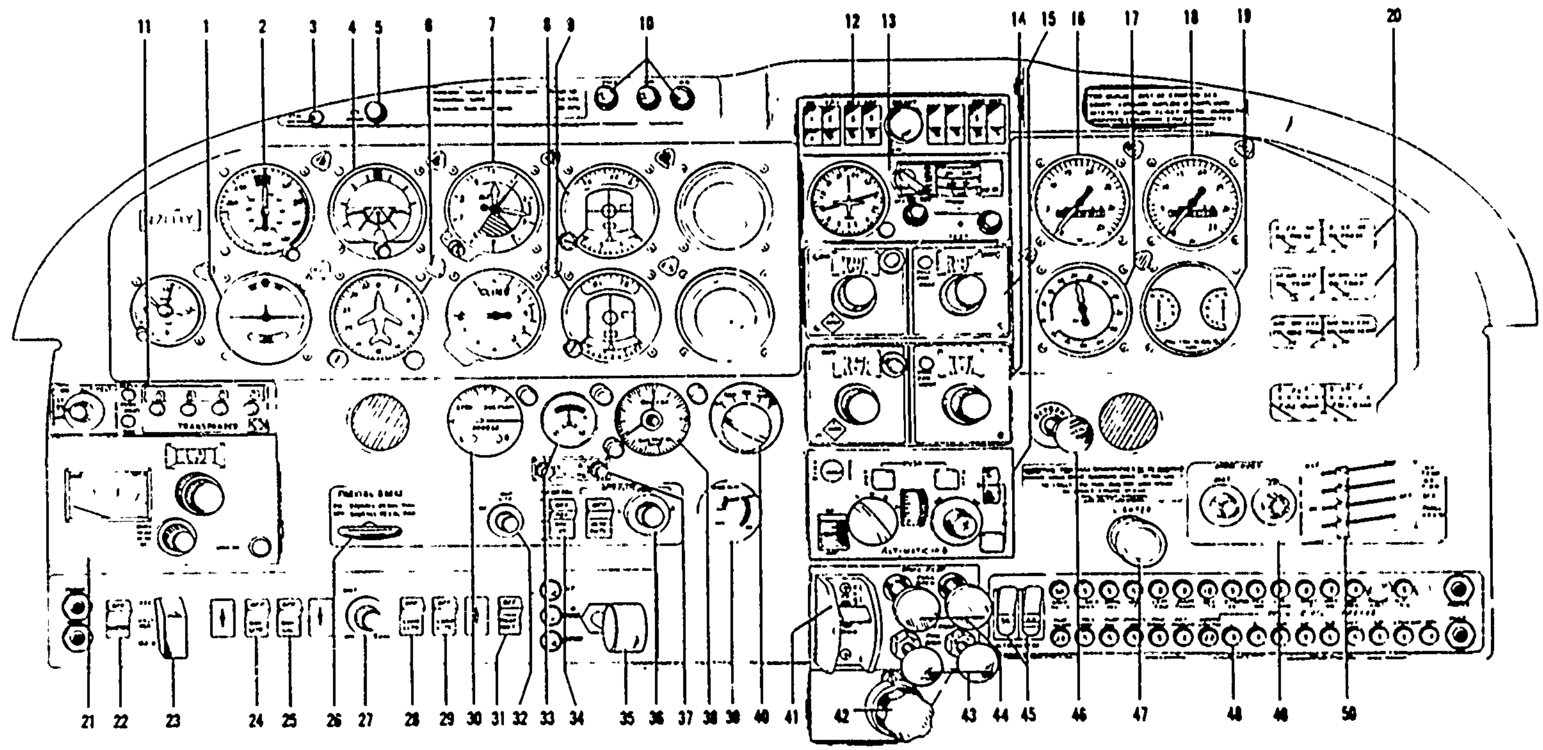

21. DME
22. MASTER SWITCH
23. VOLT. REG. SEL. SWITCH
24. NAV LIGHTS
25. ROTATING BEACON
26. PARKING BRAKE
27. POST LIGHTS SWITCH
28. LANDING LIGHT L
29. LANDING LIGHT R
30. GYRO SUCTION GAUGE
31. PITOT HEAT
32. MAP LIGHT SWITCH
33. AMMETER
34. NAV. SELECTOR SWITCH
35. LANDING GEAR SELECTOR
36. AUTOFLITE
37. ALTERNATOR TEST BUTTONS
38. MIXTURE CONTROL INDICATOR
39. FLAP INDICATOR
40. NAV/APPROACH COUPLER
41. FLAP ACTUATOR
42. RUDDER TRIM
43. ALTERNATE AIR L-R
44. COWL FLAPS L-R
45. ALTERNATOR SWITCHES
46. OXYGEN CONTROL
47. LIGHTER
48. CIRCUIT BREAKER PANEL
49. CABIN HEAT CONTROLS
50. DEFROSTER CONTROL

Figure 9. Instrument Panel Layout

REFERENCES

1. Koziol, Joseph, Manueverability of Conventional Fixed Wing Aircraft in the Landing Approach, In-House Memorandum, December 15, 1970

2. Koziol, Joseph, Selection of a Representative Light Maneuverable Aircraft for Instrumented Approach and Landing Studies, In-House Memorandum August 13, 1970

3. Koziol, Joseph, A Comparison Between the Cessna 310 and the Piper PA-30 Twin Comanche, In-House Memorandum, October 6, 1970

4. Fink, P. Marvin, and Delma C. Freeman, Jr., Full-Scale Wind-Tunnel Investigation of Static Longitudinal and Lateral Characteristics of a Light Twin-Engine Airplane, NASA TN D-4983, January, 1969.

5. Piper Twin Comanche Owner's Handbook, Part No. 753 773, January, 1970

6. Kohlman, David L., An Analytical Description of Typical Light Airplane Autopilot and Control Systems, Prepared for TSC under Purchase Order No. TS-578, December 14, 1970.